Optical Zeeman Spectroscopy of Ytterbium Monofluoride, YbF

Tongmei Ma,[†] Cleone Butler,[‡] John M. Brown,[‡] Colan Linton,[§] and Timothy C. Steimle*,[||]

School of Chemistry and Chemical Engineering, South China University of Technology, Guangzhou, 510640, People's Republic of China, Physical and Theoretical Chemistry Laboratory, Department of Chemistry, University of Oxford, South Parks Road, Oxford, OX1 3QZ, United Kingdom, Center for Laser Atomic and Molecular Science, Physics Department, University of New Brunswick, Fredericton, New Brunswick E3B 5A3, Canada, and Department of Chemistry and Biochemistry, Arizona State University, Tempe, Arizona 85287-1604

Received: April 19, 2009; Revised Manuscript Received: May 27, 2009

The Zeeman-induced shifts and splittings of low-J lines in the $^{O}P_{12}$ branch of the (0,0) band of the $A^2\Pi_{1/2}-X^2\Sigma^+$ electronic transition of a cold molecular beam sample of ytterbium monofluoride, YbF, have been recorded. The Zeeman spectra for the ^{171}YbF, ^{172}YbF, and ^{174}YbF isotopologues have been analyzed using a standard effective Hamiltonian approach. The magnetic g-factors determined for the $A^2\Pi_{1/2}(v = 0)$ state are rationalized using the predicted and observed electronic state distribution. The observed Zeeman tuning of the levels in the $A^2\Pi_{1/2}(v = 0)$ state is unexpectedly large; this is caused by mixing with the $B^2\Sigma^+$ state.

I. Introduction

It has long been realized that the various isotopologues of YbF are well suited for testing parity nonconservation (PNC)[1−4] via either the determination of the electric dipole moment (EDM) of the electron, d_e, or the interaction of the anapole moment of the Yb nuclei with the unpaired electron. Ytterbium monofluoride is a favorable case for the detection of d_e, which has been the primary focus of experimental efforts, because the strongly polarized s−p hybrid orbital of the sole unpaired electron in the $X^2\Sigma^+$ state leads to enormous internal electric fields (≈30 GV/cm)[1] along the internuclear axis. In a freely rotating molecule, this strong field averages to zero in the laboratory frame of reference. Fortunately, the closeness of the rotational levels of opposite parity of YbF and the sizable molecular electric dipole moment, μ_{el} (=3.91(4) D),[5] make it possible polarize the molecule almost completely with an external field of only moderate strength (≈10 kV/cm). A limit for d_e of $(-0.2 \pm 3.2) \times 10^{-26}$ e cm has been obtained in a relatively simple experiment that exploits the enormous internal electric field in ^{174}YbF.[6] This value can be compared with the $(7 \pm 8) \times 10^{-28}$ e cm value derived from a more elaborate experiment involving atomic Tl.[7]

The permanent electric dipole moment of the electron vanishes unless the discrete symmetries parity (P) and time reversal (T) are both violated. This P,T-odd interaction is a nuclear spin independent parity nonconservation (NSI-PNC) manifestation, and all isotopologues of YbF are relevant. Recently, DeMille et al.[8] proposed using ^{171}YbF to measure the P-odd nuclear spin-dependent parity nonconservation (NSD-PNC) effect resulting from the interaction of the anapole moment of ^{171}Yb nucleus with the unpaired electron of the $X^2\Sigma^+$ state. The nuclear anapole moment is an electric dipole moment associated with a toroidal electromagnetic current around the axis of nuclear spin and is a purely PNC manifestation.[9] In the proposed experimental scheme the $N = 0$ (+ parity) levels of the ground vibronic $X^2\Sigma^+$ ($v = 0$) state would be magnetically tuned into near degeneracy with the $N = 1$ (− parity) levels. The pairs of nearly degenerate levels are mixed by NSD-PNC interactions. A laser-induced fluorescence detection scheme using the $A^2\Pi_{1/2}-X^2\Sigma^+$ (0,0) band system is proposed; consequently, an understanding of the Zeeman tuning in both the $A^2\Pi_{1/2}$ and $X^2\Sigma^+$ states is required.

Here we report the determination of magnetic g-factors for the ^{171}YbF, ^{172}YbF, and ^{174}YbF isotopologues derived from the analysis of the Zeeman-induced shifts and splittings of the $^{O}P_{12}$ branch features of the $A^2\Pi_{1/2} \leftarrow X^2\Sigma^+$ (0,0) band. The Hamiltonian for the Zeeman effect is $\hat{H}^{Zee} = -\vec{\mu}_m \cdot \vec{B}$, where $\vec{\mu}_m$ is the magnetic moment and $\vec{B}$ is the applied magnetic field strength. Ignoring the small contribution from nonzero nuclear spins, the expectation value of $\hat{H}^{Zee}$ for a nonrotating molecule in either Hund's case (a) or (c) limit is

$$\langle \Psi^{el}; J\Omega M_J | \hat{H}^{Zee} | \Psi^{el}; J\Omega M_J \rangle = \frac{\mu_B B_Z M_J \Omega}{J(J+1)} g_e \qquad (1)$$

where it is assumed that the magnetic field is along the space fixed Z-axis, μ_B is the Bohr magneton, J is the total angular momentum, and Ω is the projection of total electronic angular momentum on the internuclear axis. The electronic g-factor, g_e, in eq 1 is the expectation value of the individual orbital and spin angular momentum operators, $\hat{\mathbf{l}}$ and $\hat{\mathbf{s}}$ operators

$$g_e \equiv \langle \Psi^{el} | \sum_i g_L T^1(\hat{l}_i) + g_S T^1(\hat{l}_i) | \Psi^{el} \rangle \qquad (2)$$

where the electronic orbital and spin g-factors g_L and g_S are 1.0 and 2.002. Thus g_e can be predicted a priori given the molecular configurations of a particular electronic state and, conversely, any proposed molecular configuration for a given electronic state must be consistent with an experimentally measured g_e. Precise modeling of the Zeeman effect requires accounting for mixing of electronic states by spin−orbit and/or rotational terms. A

* Corresponding author, Tsteimle@ASU.edu.
[†] South China University of Technology.
[‡] University of Oxford.
[§] University of New Brunswick.
[||] Arizona State University.

10.1021/jp903596g CCC: $40.75
Published on Web 06/25/2009

common procedure for the precise modeling of the energy levels of such mixed states is to transform the true Hamiltonian operator to an effective one that only operates in a given electronic state but includes the effects of the mixing terms by perturbation theory. In the effective Hamiltonian model, both g_L and g_S are allowed to deviate from 1.00 and 2.002 values of a free electron. In addition, the nonadiabatic mixing caused by $\boldsymbol{H}^{Zee}$ adds two terms g_l and g_l' (vide infra). Ignoring the rotational and nuclear spin contribution, there are four g-factors (g_S, g_L, g_l, and g_l') for a molecule in a $^{2S+1}\Pi$ state and two g-factors (g_S and g_l) for a $^{2S+1}\Sigma$ state (ref 10).

There are six naturally occurring isotopes of Yb: ^{170}Yb (3.5%), ^{171}Yb (14.3%), ^{172}Yb (21.9%), ^{173}Yb (16.1%), ^{174}Yb (31.8%), and ^{176}Yb (12.7%). The field-free spectra for the $A^2\Pi_{1/2} \leftarrow X^2\Sigma^+$ (0,0) band of all the isotopologues are now well characterized. Dunfield et al. (ref 11) recorded and analyzed the Doppler limited LIF spectrum of numerous bands in the $A^2\Pi-X^2\Sigma^+$ system of the ^{172}YbF, ^{174}YbF, and ^{176}YbF isotopologues. Soon thereafter the Hinds group[12−16] performed extensive field free and Stark studies of a molecular beam sample of ^{174}YbF. The Fourier transform microwave spectrum of the ^{174}YbF isotopologue in the $X^2\Sigma^+$ ($v = 0$) state has also been recorded and analyzed.[17] The fine structure and Yb and F hyperfine structure parameters in the $A^2\Pi_{1/2}$ ($v = 0$) and $X^2\Sigma^+$ ($v = 0$) states of the odd metal nuclear spin isotopologues ^{171}YbF and ^{173}YbF have been determined from an analysis of high-resolution laser-induced fluorescence spectrum of the (0,0) band of the $A^2\Pi_{1/2} \leftarrow X^2\Sigma^+$ transition[18] in a molecular beam sample. Prediction of the fine and fluorine hyperfine parameters for the ^{170}YbF, ^{172}YbF, and ^{176}YbF isotopologues are also given in ref 18. The only experimentally derived information on the magnetic properties of YbF is from the matrix isolation ESR measurement of ground state ^{171}YbF and ^{174}YbF.[19] The values determined for the g_S and g_l factors are 1.9975(5) and $-0.21(7) \times 10^{-2}$, respectively.

In order to interpret the data measured to test PNC, a precise knowledge of the electronic wave function in the vicinity of the Yb nucleus is required. Consequently numerous, high-level, relativistic, ab initio electronic structure calculations[20−25] for YbF in the $X^2\Sigma^+$ state have been performed. To a first approximation the $X^2\Sigma^+$ state has the sole unpaired electron in a hybridized 6s/6p/5d σ-type Yb^+-centered orbital. The hybridization is driven by the stabilization achieved from shifting the center of charge for the unpaired electron away from the electrophilic end of the Yb^+F^- molecule. Analysis of the hyperfine parameters[18] determined that the σ-type orbital is 57% 6s character, a value which is qualitatively consistent with the ab initio predictions for the $X^2\Sigma^+$ state. The measured value of the electric dipole moment ($\mu_{el} = 3.91(4)$ D[12]) for the $X^2\Sigma^+$ state, which is much smaller than a Yb^+F^- point charge distribution would suggest, is also consistent with a strongly polarized σ-type Yb^+-centered orbital. There are no published ab initio predictions for the $A^2\Pi_{1/2}$ state. Analysis of the hyperfine parameters[18] indicates that the $A^2\Pi_{1/2}$ state arises from a mixture of $Yb^+(4f^{14}\pi(6p_{\pm1}/5d_{\pm1}))F^-(2p^6)$ and $Yb^+(4f^{13}\pi(6p_{\pm1}/5d_{\pm1})\sigma(6s))F^-(2p^6)$ configurations. The significant decrease in μ_{el} upon excitation from the $X^2\Sigma^+$ state to the $A^2\Pi_{1/2}$ state (μ_{el} (=2.46(3) D)[14] suggests that the $Yb^+(4f^{13}\pi(6p_{\pm1}/5d_{\pm1})\sigma(6s))F^-(2p^6)$ configuration is significant because the promotion of an electron from the compact 4f orbital to a diffuse, highly polarizable, π ($6p_{\pm1}$/$5d_{\pm1}$) orbital will reduce μ_{el}. The g_e-factor for a molecule in Hund's case (a) $^2\Pi_{1/2}$ state is expected to be zero. If a nonzero value is determined experimentally, it will provide insight into the nature of the $A^2\Pi_{1/2}$ state.

II. Experimental Section

The supersonic molecular beam production and laser-induced fluorescent detection schemes are identical to those used in the previous field-free measurements of YbF.[18] A continuously rotating ytterbium metal rod was ablated in a supersonic expansion of 1−3% sulfur hexafluoride (SF_6) seeded in argon carrier gas with a backing pressure of approximately 200 psi. The pulsed free jet expansion was skimmed to form a well-collimated molecular beam which was crossed with a single longitudinal mode, continuous wave dye laser approximately 50 cm downstream from the source. The laser power was attenuated to approximately 30 mW and lightly focused to avoid power broadening. Spectral line widths of less than 40 MHz full width at half-maximum (fwhm) were obtainable by this combination of beam collimation and low laser power. The relative wavelengths were measured by simultaneously recording the transmission through an actively stabilized, calibrated, confocal etalon.

A homogeneous magnetic field was generated using a homemade electromagnet in the interaction region of molecular beam and laser.[26] The electromagnet consisted of a pair of Helmholtz coils with ferromagnetic poles through which 5 mm holes were drilled to allow for the passage of the molecular beam. The field was calibrated using a commercial gaussmeter. A polarization rotator was used to align the electric field vector of the linearly polarized laser radiation either perpendicular or parallel to the static magnetic field vector. The combined systematic error associated with the measurement of the magnetic field induced frequency shifts, and the field strength is estimated to be less than 2%.

III. Observations

(a) ^{172}YbF and ^{174}YbF. The low-J lines in the $^OP_{12}$ branch of the (0,0) $A^2\Pi_{1/2}-X^2\Sigma^+$ band were selected for the Zeeman measurement because these branch features are unblended, relatively intense, and involve levels of low angular momenta. The branch designation used here is the conventional $^{\Delta N}\Delta J_{F_i'F_i''}$ scheme in which the F''_i and F'_i subscripts are the spin component labels for the $X^2\Sigma^+$ and $A^2\Pi_{1/2}$ states, respectively. This scheme, which is most appropriate for a $^2\Pi$ (Hund's case $a_{\beta J}$)$-^2\Sigma^+$ (Hund's case $b_{\beta J}$) transition, has been used for YbF even though the energy level pattern for the low-rotational levels of the $X^2\Sigma^+$ state, particularly for the odd Yb nuclear spin isotopologues, is closer to a Hund's case $b_{\beta S}$ limit. The spectra for the $^OP_{12}(2)$ transition of the ^{172}YbF isotopologue recorded field-free and in the presence of a 468 G magnetic field oriented perpendicular ($\Delta M_F = \pm1$) to the field of the laser radiation are presented in left-hand portion of Figure 1. The Zeeman spectrum of the ^{172}YbF isotopologue is overlapped by features from the ^{174}YbF isotopologue. The predicted Zeeman spectrum for the ^{172}YbF isotopologue, also given in Figure 1, was generated using the optimized g-factors, details of which are given below. A line width at half-maximum (fwhm) of 30 MHz was used in the prediction, which is slightly less than the observed 40 MHz fwhm line widths.

The associated energy level pattern as a function of magnetic field strength and the Zeeman spectral assignments are given in right-hand portion of Figure 1. The field-free $^OP_{12}(2)$ branch feature of the ^{172}YbF isotopologue consists of two closely spaced transitions ($F' = 1 \leftarrow G'' = 0$; $F'' = 2$ ($\nu = 18104.8285$ cm^{-1}) and $F' = 1 \leftarrow G'' = 1$; $F'' = 2$ ($\nu = 18104.8347$ cm^{-1})) because the $N = 2$ rotational level of the $X^2\Sigma^+$ state is split into a doublet by the $^{19}F(I = 1/2)$ magnetic hyperfine interaction. The splitting is approximately 170 MHz ($\approx b_F(F)$) and the two groups are

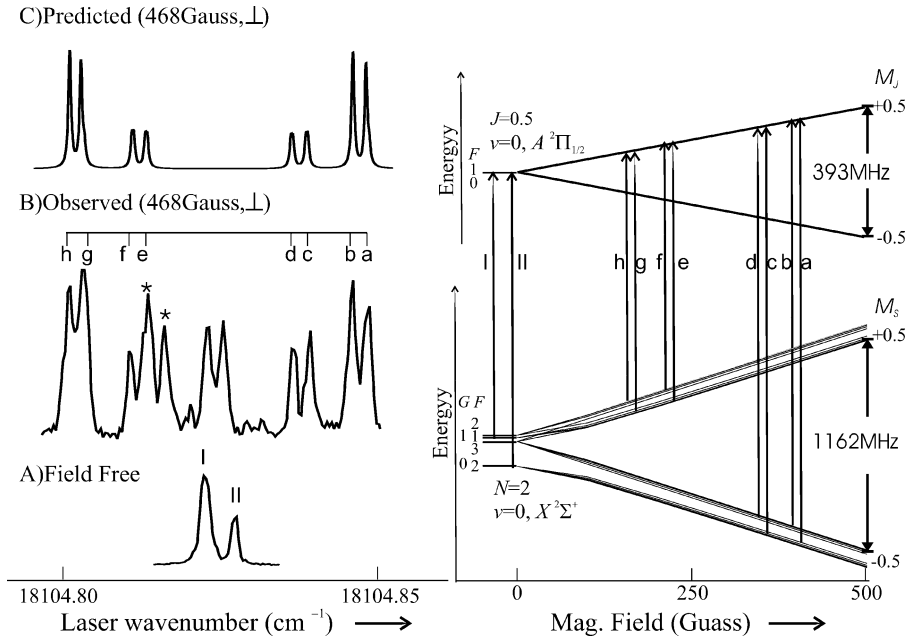

Figure 1. The $^{O}P_{12}(2)$ transition of the ^{172}YbF isotopologue recorded field free and in the presence of a 468 G magnetic field oriented perpendicular ($\Delta M_F = \pm 1$) to the field of the laser radiation and associated energy level pattern as a function of applied field. The Zeeman features marked by asterisks are from the ^{174}YbF isotopologue.

labeled by intermediate quantum numbers G (where $\boldsymbol{G} = \boldsymbol{I} + \boldsymbol{S}$). There is a very small splitting (<10 MHz) between the $F = 1$, 2, and 3 levels associated with the $G = 1$ level due to the rotation induced uncoupling of the nuclear spin from the electron spin. The ^{19}F($I = 1/2$) magnetic hyperfine splitting in the $J = 0.5$ level of the $A^2\Pi_{1/2}$ is not resolved and the $F' = 1$ and 2 field-free levels are indicated as degenerate in Figure 1.

The electron spin and nuclear spin are weakly coupled to the molecular axis in the $N = 2$ rotational level of the $X^2\Sigma^+$ state and the appropriate approximately good quantum numbers upon application of the magnetic field are the projection quantum numbers $M_S(= \pm 1/2)$ and M_I ($=\pm 1/2$). The level pattern consists of four groups of levels associated with the four possible combinations of M_I and M_S. The electron spin is strongly coupled to the molecular axis in the $A^2\Pi_{1/2}$ state via spin−orbit interaction and the appropriate projection quantum numbers are M_J ($=\pm 1/2$) and M_I ($= \pm 1/2$) for the field strengths used. The Zeeman tuning of the $J = 0.5$ levels in the $A^2\Pi_{1/2}$ state is relatively weak compared with the tuning of the $N = 2$ level in the $X^2\Sigma^+$ state and is identically zero in the Hund's case a limit.

Measurements have also been made for the ^{174}YbF isotopologue. The energy level scheme is essentially the same as that for ^{172}YbF.

(b) ^{171}YbF. The spectra associated with the $G = 0$ levels of the $^{O}P_{12}(2)$ branch ($\nu = 18105.0340$ cm^{-1}) feature for the ^{171}YbF isotopologue recorded field-free and in the presence of a 641 G magnetic field oriented perpendicular to the field of the laser radiation ($\Delta M_F = \pm 1$) are presented in the left-hand side of Figure 2. The ^{171}Yb($I = 1/2$) magnetic hyperfine interaction in the $X^2\Sigma^+$ state is approximately a factor of 20 larger than that for ^{19}F($I = 1/2$) and the appropriate vector coupling can be written as

$$\boldsymbol{S} + \boldsymbol{I}_1 = \boldsymbol{G}; \qquad \boldsymbol{N} + \boldsymbol{G} = \boldsymbol{F}_1; \qquad \boldsymbol{F}_1 + \boldsymbol{I}_2 = \boldsymbol{F} \tag{3}$$

where $\mathbf{I}_1$ and $\mathbf{I}_2$ are the nuclear spins for ^{171}Yb and ^{19}F, respectively. The $G = 0$ levels are approximately 7 GHz ($\approx b_F(^{171}\text{Yb})$) lower in energy than the $G = 1$ levels which are not shown in Figure 2. The ^{19}F ($I = 1/2$) hyperfine splitting is not observed either in the $J = 0.5$ levels of the $A^2\Pi_{1/2}$ state or in the $N = 2$, $G = 0$ levels of the $X^2\Sigma^+$ state so the appropriate quantum number for the levels in Figure 2 is F_1 for both states. The field-free $J = 0.5$, $F_1 = 1 \leftarrow N = 2$, $G = 0$, $F_1 = 2$ transition of Figure 2, which appears as a single spectral feature, actually consists of numerous unresolved transitions.

The magnetic tuning of the energy levels associated with the $J = 0.5$, $F_1 = 1 \leftarrow N = 2$, $G = 0$, $F_1 = 2$ transition is presented on the right-hand side of Figure 2. The single field-free spectral feature splits into three unequally spaced components upon application of the magnetic field. The centroid of the three features shifts to higher frequency because $N = 2$, $G = 0$ levels of the $X^2\Sigma^+$ state are all shifted to lower energy due to interaction with the $N = 2$, $G = 1$ levels. The splitting into three components is caused by the splitting of the $F_1 = 1$ level into the $M_{F_1} = 0$ and ± 1 components. The ^{171}Yb nuclear spin is not strongly decoupled from the molecular axis in the $A^2\Pi_{1/2}$ state for the fields used because of the large $b_F(^{171}\text{Yb})$ interaction and M_{F_1} is the appropriate labeling quantum number. The $M_{F_1} = 0$ component exhibits a second-order effect due to mixing with the $F_1 = 0$, $M_{F_1} = 0$ level producing an unequal splitting.

A total of 49 Zeeman shifted components for the ^{172}YbF isotopologue, 50 shifted components for the ^{174}YbF isotopologue, and 378 shifted components for the ^{171}YbF isotopologue were recorded at field strengths ranging from 123 to 882 G for the (0,0) $A^2\Pi_{1/2}-X^2\Sigma^+$ band system. The measured shifts, assignments, and the differences between the observed and calculated shifts are available as Supporting Information.[27]

IV. Analysis

The field-free energy levels were modeled using the effective Hamiltonian and parameters from the previous analysis.[18] The field-free spectroscopic parameters for the ($v = 0$) $X^2\Sigma^+$ and ($v = 0$) $A^2\Pi_{1/2}$ states are reproduced for

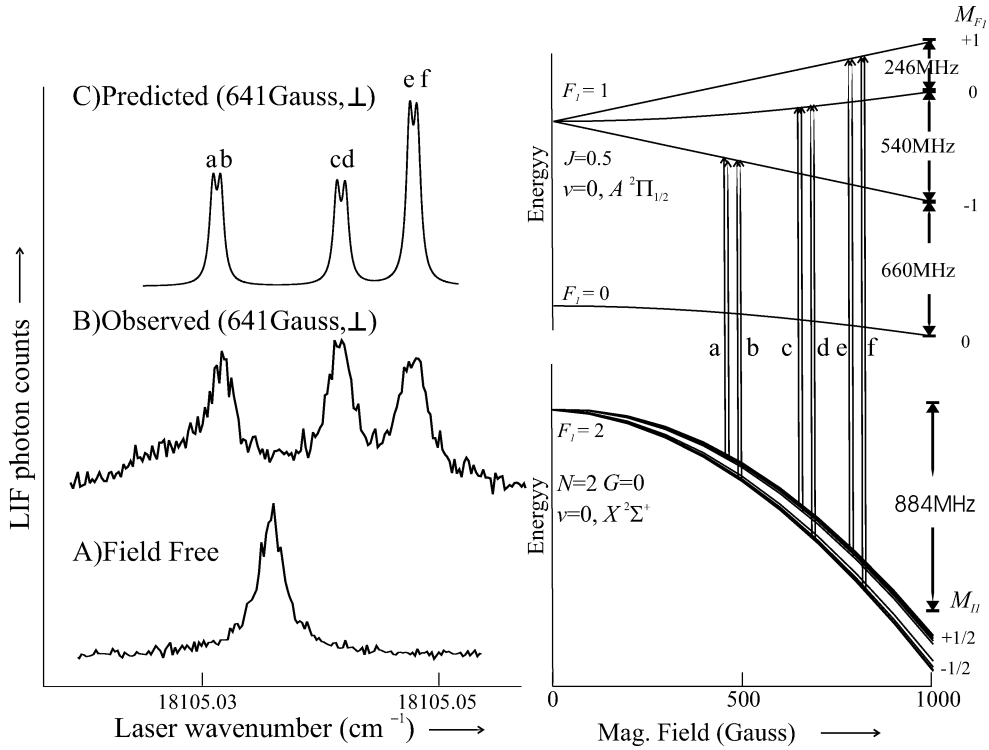

Figure 2. The $^{O}P_{12}(2)$ transition of the ^{171}YbF isotopologue recorded field-free and in the presence of a 641 G magnetic field oriented perpendicular ($\Delta M_F = \pm 1$) to the field of the laser radiation and associated energy level pattern as a function of applied field. The ^{19}F($I = 1/2$) hyperfine splitting is not resolved and the approximately good field-free quantum number for $X^2\Sigma^+$ and $A^2\Pi_{1/2}$ states is F_1.

TABLE 1: Spectroscopic Parameters Used To Model the Field-Free Energies of the $X^2\Sigma^+(v = 0)$ and $A^2\Pi_{1/2}(v = 0)$ States of ^{171}YbF, ^{172}YbF, and ^{171}YbF (cm^{-1})[a]

state	parameter	^{171}YbF	^{172}YbF	^{174}YbF
$X^2\Sigma^+$ ($v = 0$)	B	0.2417118	0.2415712	0.2412945
	10^6D	0.23920	0.23906	0.23879
	$10^3\gamma$	−0.44831	−0.44805	−0.44753
	b_F(Yb)	0.24214	N/A	N/A
	c(Yb)	0.0085	N/A	N/A
	b_F(F)	0.005679	0.005679	0.005679
	c(F)	0.002849	0.002849	0.002849
$A^2\Pi_{1/2}$ ($v = 0$)	A	1365.3000	1365.3000	1365.3000
	10^3A_D	1.1864	1.1864	1.1864
	B	0.2480568	0.2479112	0.2476292
	10^6D	0.20326	0.20323	0.19948
	$(p + 2q)$	−0.39762	−0.39747	−0.39707
	$h_{1/2}$(Yb)	0.0122	N/A	N/A
	d(Yb)	0.03323	N/A	N/A
	T_0	18788.6502	18788.8760	18788.8461

[a] From ref 18.

convenience in Table 1 Briefly, a 4 × 4 or 8 × 8 matrix representation in a Hund's case $a_{\beta J}$ basis set, $|\eta\Lambda\rangle|S\Sigma\rangle|J\Omega(JI)F\rangle$, was constructed and diagonalized to produce the eigenvalues and eigenvectors for the $X^2\Sigma^+$ ($v = 0$) and $A^2\Pi_{1/2}$ ($v = 0$) states, respectively, for the ^{172}YbF and ^{174}YbF isotopologues. For the ^{171}YbF isotopologue, 8 × 8 and 16 × 16 matrix representations in a sequentially coupled Hund's case $a_{\beta J}$ basis set, $|\eta\Lambda\rangle|S\Sigma\rangle|J\Omega(JI_1)F_1(F_1I_2)F\rangle$, were constructed and diagonalized to produce the eigenvalues and eigenvectors for the $X^2\Sigma^+$ ($v = 0$) and $A^2\Pi_{1/2}$ ($v = 0$) states, respectively. Although the ^{19}F hyperfine splitting was not resolved in the ($v = 0$) $A^2\Pi_{1/2}$ state, it was included in the basis set and matrix representations to facilitate the spectral prediction procedure.

It is evident from Figures 1 and 2 that the magnetic field induced mixing of the fine and hyperfine components of a given rotational level needs to be considered to account for the observed nonlinear spectral shifts. The effective Zeeman Hamiltonian was taken as[10,28]

$$\hat{\mathbf{H}}^{\mathrm{Zee}}(\mathrm{eff}) = g_S\mu_B\hat{\mathbf{S}}\cdot\hat{\mathbf{B}} + g'_L\mu_B\hat{\mathbf{L}}\cdot\hat{\mathbf{B}} + g_l\mu_B(\hat{S}_x\hat{B}_x + \hat{S}_y\hat{B}_y) + g'_l\mu_B(e^{-2i\phi}\hat{S}_+\hat{B}_+ + e^{+2i\phi}\hat{S}_-\hat{B}_-) \quad (4)$$

The expressions for the matrix elements for a single nuclear spin Hund's case ($a_{\beta J}$) basis function, $|\eta\Lambda\rangle|S\Sigma\rangle|J\Omega(JI)F\rangle$, can be found in refs 10 and 29. The expressions for the two nuclear spin Hund's case $a_{\beta J}$ basis function, $|\eta\Lambda\rangle|S\Sigma\rangle|J\Omega(JI_1)F_1(F_1I_2)F\rangle$, are readily obtained by using standard angular momentum theory for coupling of the second nuclear spin.[30] Although in the final analysis a Hund's case $a_{\beta J}$ basis function was used to construct the matrix representation of $\hat{\mathbf{H}}^{\mathrm{Zee}}$(eff), initial modeling of the Zeeman effect for the $X^2\Sigma^+$ ($v = 0$) state was performed by using the diagonal elements of the representation of the operator in a Hund's case $b_{\beta S}$ basis set. The matrix elements of $\hat{\mathbf{H}}^{\mathrm{Zee}}$(eff) in a Hund's case $b_{\beta S}$ basis set for a molecule in Σ electronic state are given in Appendix A.

The matrix representation of the Zeeman Hamiltonian operator is diagonal in M_F, the projection of total angular momentum, but of infinite dimension. The energies of the levels associated with the $^{O}P_{12}(2)$, $^{O}P_{12}(3)$, and $^{O}P_{12}(4)$ lines were matched to the level of accuracy of the experiment (≈20 MHz) by truncating the matrix representation to include $F = 0$ through $F = 5$ for both the $X^2\Sigma^+$ ($v = 0$) and $A^2\Pi_{1/2}$ ($v = 0$) states for the ^{172}YbF and ^{174}YbF isotopologues and $F = 0.5$ through $F = 5.5$ for ^{171}YbF. A nonlinear least-squares fitting program was used to reduce the data. The input data to the fitting program were the observed shifts (Supporting Information) and initial guess of the magnetic g-factors. The signal to-noise of the ^{171}YbF isotopologue data was better

TABLE 2: Fitted Zeeman Parameters of ^{171}YbF, ^{172}YbF, and ^{174}YbF

fits[a]	g_L ($A^2\Pi_{1/2}$)	g_l' ($A^2\Pi_{1/2}$)	std dev (MHz)
fit A	0.996(8)[b]	−0.8016	14.7
fit B[c]	1.118(16)	−0.722(9)	12.6

[a] In all fits $g_S(X^2\Sigma^+)$ and $g_l(X^2\Sigma^+)$ are constrained to 2.0023 and 9.4×10^{-4}; $g_l(A^2\Pi_{1/2})$ is constrained to 0. [b] The numbers in parentheses represents a 2σ statistical error estimate. [c] Correlation coefficient = 0.904.

than that of the ^{172}YbF and ^{174}YbF isotopologues due to more extensive signal averaging and was weighted twice as much in the fitting. The data are not extensive enough to fit all possible six *g*-factors (g_S and g_l for the $X^2\Sigma^+$ state and g_L, g_S, g_l' and g_l for the $A^2\Pi_{1/2}$ state). It is expected that $g_l(A^2\Pi_{1/2})$ will be very small, and it was constrained to zero. The prediction using $g_S = 2.0023$ for the $X^2\Sigma^+$ and $A^2\Pi$ states, $g_L(A^2\Pi_{1/2}) = 1.000$, $g_l(X^2\Sigma^+)$ and $g_l'(A^2\Pi_{1/2})$ constrained to the values predicted by the Curl-type relationships: $g_l = -\gamma/2B = 9.4 \times 10^{-4}$; $g_1' = p/2B = -0.8016$ gives a residual of 14.9 MHz. The isotopologue average value for B, γ, and $p + 2q$ were used and it was assumed that $2q$ was negligible compared to p. Fits using various combinations of the *g*-factors were attempted. Whereas the electronic spin *g*-factor, g_S, of the effective Hamiltonian for the ($v = 0$) $X^2\Sigma^+$ state is expected to be very close to the free electron value of 2.0023, the orbital *g*-factor, g_L' for the ($v = 0$) $A^2\Pi_{1/2}$ state is expected to differ from unity because of nonadiabatic contributions and g_L' was varied in all fits. In the end the *g*-factors for the $X^2\Sigma^+$ state were constrained to $g_S = 2.0023$ and $g_l = 9.27 \times 10^{-4}$. A single parameter fit ("fit A" Table 2) was performed in which $g_L'(A^2\Pi_{1/2})$ was varied and $g_S(A^2\Pi_{1/2})$ and $g_l'(A^2\Pi_{1/2})$ were constrained to 2.0023 and $= -0.8016$. The residual of the single parameter fit is 14.6 MHz, and the optimized value for $g_L'(A^2\Pi_{1/2})$ is 0.996(8). A two-parameter fit ("fit B" Table 2) was performed in which both g_L' and g_l' for the $A^2\Pi_{1/2}$ state were varied. The residual of the two-parameter fit is 12.6 MHz, and the optimized value for $g_L'(A^2\Pi_{1/2})$ and $g_l'(A^2\Pi_{1/2})$ are 1.118(16) and −0.722(9). The numbers in parentheses represent a 2σ estimate of the statistical error. The inclusion of the g_l' parameter in the Zeeman operator is essential for modeling magnetic tuning in the ($v = 0$) $A^2\Pi_{1/2}$ state.

The quantum number assignments for the LIF spectra were greatly assisted by simulations of the spectra. These simulations were achieved by setting up the matrix of transition moments in a Hund's case $a_{\beta J}$ coupling scheme and transforming it by the eigenvectors for the upper and lower states

$$\boldsymbol{\mu}(\text{exact}) = \mathbf{EV}(X^2\sum^+)\boldsymbol{\mu}(\text{Hund's case}(a_{\beta J}))\mathbf{EV}(A^2\Pi_{1/2}) \quad (5)$$

The transition moments, $\boldsymbol{\mu}$(exact), were then squared, multiplied by the Boltzmann factor for an estimated temperature of 20 K, and used in conjunction with a Lorentzian line width of 30 MHz fwhm to predict each spectral feature.

V. Discussion

The Zeeman effect in the low rotational levels of YbF in the $X^2\Sigma^+$ state studied here ($N = 2$, 3, and 4) is that expected for an isolated $^2\Sigma^+$ state (i.e. $g_S = 2.0023$). The g_l term, which accounts for anisotropic contributions, is small and consistent with the small spin-rotation parameter, γ. It has been shown[12] that γ ($X^2\Sigma^+$) exhibits a strong rotational dependence and it may be expected that the Zeeman effect in the higher rotational levels will be more difficult to model. The strong rotational dependence of γ ($X^2\Sigma^+$) is due to the rotational induced mixing of the $X^2\Sigma^+$ state with other low-lying states. The dominant configuration for the $X^2\Sigma^+$ state results from coupling $Yb^+(4f^{14}6s^1)$ with $F^-(2s^22p^6)$ accompanied by 6s/6p hybridization: $([Xe]4f^{14})_{Yb}[He]_F\sigma_{F2s}{}^2\sigma_{F2p}{}^2\pi_{F2p}{}^4\sigma_{Yb6s6p}{}^1$. The coupling of the excited $Yb^+(4f^{13}6s^2)$ configuration with $F^-(2s^22p^6)$ produces $^2\Sigma^+$, $^2\Pi_r$, $^2\Delta$, and $^2\Phi$ states at approximately 7000 cm^{-1} above the $X^2\Sigma^+$.[19,20] Mixing with these states will cause the g_S-factor of the $X^2\Sigma^+$ to be lower than 2.0023. Mixing with an excited state of $^4\Sigma^-$ symmetry would have the effect of lowering the g_S-factor from that of a free electron, but no such state has been either detected or predicted.

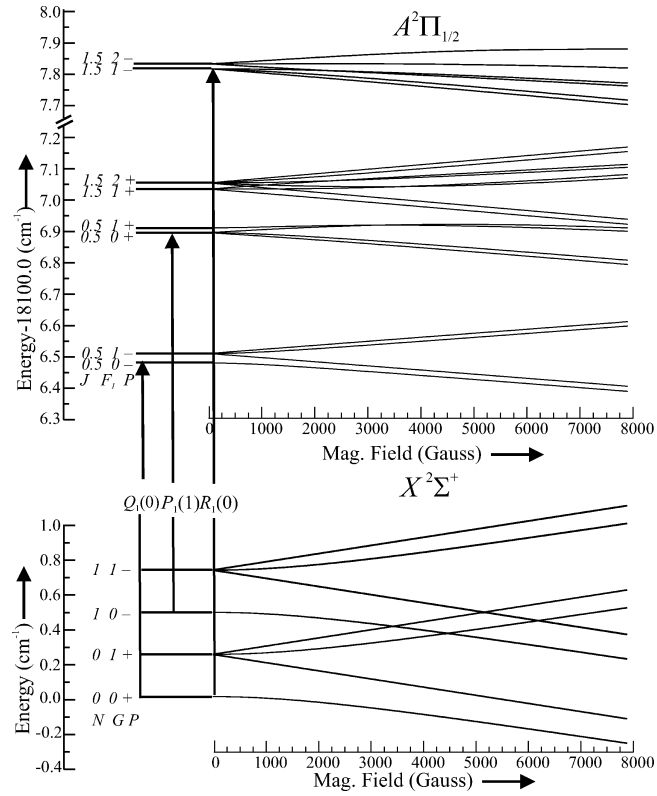

Figure 3. The low rotational levels of the $X^2\Sigma^+$ and $A^2\Pi_{1/2}$ states for the ^{171}YbF isotopologue as a function of applied magnetic field. The small ^{19}F hyperfine spitting is not discernible in the plots. The $G = 1$, $N = 0$ (+ parity) levels of the ground vibronic $X^2\Sigma^+$ ($v = 0$) state is magnetically tuned into near degeneracy with the $G = 0$, $N = 1$ (− parity) levels at approximately 3300 and 4500 G. The approximately good quantum number at high magnetic field is M_S (= ±1/2), $M_I(^{171}\text{Yb})$ (= ±1/2) and $M_I(^{19}\text{F})$ (= ±1/2).

The Zeeman tuning of the $A^2\Pi_{1/2}$ state is much larger than that expected for an isolated $^2\Pi$ state. The rotational and spin−orbit mixing of the $A^2\Pi_{1/2}$ ($v = 0$) state with the $B^2\Sigma^+$ ($v = 0$) state, which is approximately 2950 cm^{-1} above $A^2\Pi_{1/2}$ ($v = 0$),[11] is most likely the cause of the enhanced tuning. The interaction between the vibronic levels of these two states has been shown to be responsible for the large Λ-doubling in the for the $A^2\Pi_{1/2}$ ($v = 0$) state ($p + 2q \approx -0.4$ cm^{-1}) and thus responsible for the large value of g_l'.

VI. Conclusion

The magnetic tuning of the low-*J* branch features of the (0,0) band of the $A^2\Pi_{1/2}-X^2\Sigma^+$ electronic transition has been

analyzed and accurately modeled. The results will be useful in designing the proposed NSD-PNC experiment[8] in which the $N = 0$ (+ parity) levels of the ground vibronic $X^2\Sigma^+$ ($v = 0$) state of ^{171}YbF will be magnetically tuned into near degeneracy with the $N = 1$ (− parity) levels and monitored using the $R_1(0)$, $Q_1(0)$, or $P_1(1)$ lines. The magnetic tuning of the low-J rotational lines for the $A^2\Pi_{1/2}$ and $X^2\Sigma^+$ states of the ^{171}YbF isotopologue are given in Figure 3, and the $G = 0$ component of the $R_1(0)$ ($\nu = 18107.83$ cm^{-1})), $Q_1(0)$ ($\nu = 18106.49$ cm^{-1})), or $P_1(1)$ ($\nu = 18106.39$ cm^{-1})) lines indicated. The tuning pattern for the $X^2\Sigma^+$ state reveals that the approximately good quantum number at high magnetic field is M_S (=±1/2), M_I(^{171} Yb) (=±1/2) and M_I(^{19}F) (=±1/2), whereas at low and moderate field they are M_G (=0,±1). The $G = 1$, $M_G = +1$, $N = 0$ (+ parity) and $G = 1$, $M_G = 0$, $N = 0$ (+ parity) levels of the ground vibronic $X^2\Sigma^+$ ($v = 0$) state are magnetically tuned into near degeneracy with the $G = 0$, $M_G = 0$, $N = 1$ (− parity) level at approximately 3300 and 4500 G, respectively.

Appendix A. Matrix Elements of the Zeeman Hamiltonian for a Molecule in a $^{2S+1}\Sigma$ Electronic State in a Hund's Case $b_{\beta S}$ Basis Set. Ignoring nuclear spin and rotational contributions, the Zeeman operator for a $^{2S+1}\Sigma$ state written in spherical tensor form is

$$\hat{\mathbf{H}}^{\mathrm{Zee}}(\mathrm{eff}) = g_S \mu_B S_Z B_Z - \mu_B B_Z \sum_{k=0,2} (-1)^k [(2k+1)/3]^{1/2} T_{p=0}{}^1(g_l{}^k, S) \quad \text{(A1)}$$

where $T_{p=0}{}^1(g_l{}^k,S)$ represents the tensor product in space fixed coordinates

$$T_{p=0}{}^1(g_l{}^k, S) = -(3)^{1/2} \sum_{p_1} \begin{pmatrix} 1 & k & 1 \\ 0 & p_1 & -p_1 \end{pmatrix} T_{-p_1}{}^k(g_l) T_{p_1}{}^1(S) \quad \text{(A2)}$$

The spherical tensor anisotropic g-factors in the molecule axis are related to the principal axis components by

$$T_{q=0}{}^0(g_l) = -(3)^{-1/2}(g_l{}^{aa} + 2g_l{}^{bb}) \quad \text{(A3)}$$

$$T_{q=0}{}^2(g_l) = (2/3)^{-1/2}(g_l{}^{aa} - g_l{}^{bb}) \quad \text{(A4)}$$

The conventional anisotropic correction parameter g_l given in eq 1 is equal to$g_l{}^{bb}$. The $g_l{}^{aa}$ term has not been previously considered.

Matrix elements in Hund's case $b_{\beta S}$ can be derived using standard spherical tensor algebra[9,29]

Term 1:

$$\langle N';SIG';F'M_F'|g_S\mu_B S_Z B_Z|N;SIG;FM_F\rangle = \delta_{M_F M_F}\delta_{N'N} g_S \mu_B B_Z (-1)^{F'-M_F} \begin{pmatrix} F' & 1 & F \\ -M_F & 0 & M_F \end{pmatrix} \times (-1)^{F'+N+G+1}[(2F'+1)(2F+1)]^{1/2} \begin{Bmatrix} G' & F' & N \\ F & G & 1 \end{Bmatrix} \times (-1)^{G+S+I+1}[(2G'+1)(2G+1)]^{1/2} \begin{Bmatrix} S & G' & I \\ G & S & 1 \end{Bmatrix} \times [S(S+1)(2S+1)]^{1/2} \quad \text{(A5)}$$

Term 2:

$$\langle N';SIG';F'M_F'|\mu_B B_Z \sum_{k=0,2} (-1)^k[(2k+1)/3]^{1/2} T_{p=0}{}^1(g_l{}^k, S) \times |N;SIG;FM_F\rangle = -\delta_{M_F M_F}\mu_B B_Z (-1)^{F'-M_F} \begin{pmatrix} F' & 1 & F \\ -M_F & 0 & M_F \end{pmatrix} \times \sum_{k=0,2} (-1)^k (2k+1)^{1/2}[(2F'+1)(2F+1)]^{1/2} \times \begin{Bmatrix} N' & N & k \\ G' & G & 1 \\ F' & F & 1 \end{Bmatrix} (-1)^{G+S+I+1}[(2G'+1)(2G+1)]^{1/2} \times \begin{Bmatrix} S & G' & I \\ G & S & 1 \end{Bmatrix} [S(S+1)(2S+1)]^{1/2} \sum_q (-1)^{N'-\Lambda'} \times \begin{pmatrix} N' & k & N \\ -\Lambda' & q & \Lambda \end{pmatrix} [(2N+1)(2N+1)]^{1/2} \langle \acute{a}\eta\Lambda'|T_q{}^k(g_l)|\eta\Lambda\rangle \quad \text{(A6)}$$

The terms associated with g_S and $T_{q=0}{}^0(g_l)$ are totally correlated and there are only two determinable g-factors for a $^{2S+1}\Sigma$ state which are usually taken as g_S and g_l (=$g_l{}^{bb}$).

Acknowledgment. This research has been supported by the National Science Foundation—Experimental Physical Chemistry (Grant No.0646473) and by the Natural Sciences and Engineering Research Council (NSERC) of Canada.

Supporting Information Available: A table of observed and differences between the observed and calculated Zeeman shifts and the associated quantum number assignments. This material is available free of charge via the Internet at http://pubs.acs.org.

References and Notes

(1) Kozlov, M. G.; Ezhov, V. F. *Phys. Rev. A* **1994**, *49*, 4502.
(2) Titov, A. V.; Mosyagin, N. S.; Ezhov, V. F. *Phys. Rev. Lett.* **1996**, *77*, 5346.
(3) Hinds, E. A. *Phys. Scr.* **1997**, *T70*, 34.
(4) Mosyagin, N. S.; Kozlov, M. G.; Titov, A. V. *J. Phys. B: At. Mol. Phys.* **1998**, *31*, L763.
(5) Sauer, B. E.; Wang, J.; Hinds, E. A. *J. Chem. Phys.* **1996**, *105*, 7412.
(6) Hudson, J. J.; Sauer, B. E.; Tarbutt, M. R.; Hinds, E. A. *Phys. Rev. Lett.* **2002**, *89*, 023103-1.
(7) Regan, B. C.; Commins, E.; Schmidt, C.; DeMille, D. *Phys. Rev. Lett.* **2002**, *88*, 71805-4.
(8) DeMille, D.; Cahn, S. B.; Murphree, D.; Rahmlow, D. A.; Kozlov, M. G. *Phys. Rev. Lett.* **2008**, *100*, 023008.
(9) Haxton, W. C.; Wieman, C. E. *Annu. Rev. Nucl. Phys.* **2001**, *51*, 261.
(10) Brown, J. M. ; Carrington, A. *Rotational Spectroscopy of Diatomic Molecules*; Cambridge University Press: Cambridge, 2003.
(11) Dunfield, K. L.; Linton, C.; Clarke, T. E.; McBride, J.; Adam, A. G.; Peers, J. R. D. *J. Mol. Spectrosc.* **1995**, *174*, 433.
(12) Sauer, B. E.; Wang, J.; Hinds, E. A. *Phys. Rev. Lett.* **1995**, *74*, 1554.
(13) Sauer, B. E.; Wang, J.; Hinds, E. A. *J. Chem. Phys.* **1996**, *105*, 7412.
(14) Sauer, B. E.; Cahn, S. B.; Kozlov, M. G.; Redgrave, G. D.; Hinds, E. A. *J. Chem. Phys.* **1999**, *110*, 8424.
(15) Condylis, P. C.; Hudson, J. J.; Tarbutt, M. R.; Sauer, B. E.; Hinds, E. A. *J. Chem. Phys.* **2005**, *123*, 131101.
(16) Tarbutt, M. R.; Hudson, J. J.; Sauer, B. E.; Hinds, E. A.; Ryzhov, V. A.; Ryabov, V. L.; Ezhov, V. F. *J. Phys. B.: At. Mol. Phys.* **2002**, *35*, 5013.
(17) Dickinson, C. S.; Coxon, J. A.; Walker, N. R.; Gerry, M. C. L. *J. Chem. Phys.* **2001**, *115*, 6979.
(18) Steimle, T. C.; Ma, T.; Linton, C. *J. Chem. Phys.* **2008**, *127*, 234316. Steimle, T. C.; Ma, T.; Linton, C. *J. Chem. Phys.* **2008**, *128*, 209903/1.
(19) Van Zee, R. J.; Seely, M. L.; DeVore, T. C.; Weltner, W., Jr. *J. Phys. Chem.* **1978**, *82*, 1192.
(20) Dolg, M.; Stoll, H.; Preuss, H. *Chem. Phys.* **1992**, *165*, 21.
(21) Liu, W.; Dolg, M.; Li, L. *J. Chem. Phys.,* **1998**, *108*, 2886.

(22) Parpia, F. A. *J. Phys. B: At. Mol. Phys.* **1998**, *31*, 1409–1431.
(23) Quiney, H. M.; Skaane, H.; Grant, I. P. *J. Phys. B.: At. Mol. Phys.* **1998**, *31*, L85.
(24) Titov, A. V.; Mosyagin, N. S.; Petrov, A. N.; Isaev, T. A. *Int. J. Quantum Chem.* **2005**, *104*, 223.
(25) Nayak, M. K.; Chaudhuri, R. K. *Chem. Phys. Lett.* **2006**, *419*, 191.
(26) Steimle, T. C.; Gengler, J.; Chen, J. *Can. J. Chem.* **2004**, *82*, 779.
(27) Available free of charge via the Internet at http://pubs.acs.org.
(28) Weltner, W., Jr. *Magnetic Atoms and Molecules*; Dover Publications, Inc.: New York, 1983.
(29) Chen, J.; Gengler, J.; Steimle, T. C.; Brown, J. M. *Phys. Rev. A* **2006**, *73*, 012502.
(30) Edmonds, E. D. *Angular Momentum in Quantum Mechanics*; Princeton University Press: Princeton, NJ, 1960.

JP903596G